Research Article Vol. 33, No. 22 / 3 Nov 2025 / Optics Express 45574
Optics EXPRESS

Effect of flux on the spark-plasma-sintering (SPS) of translucent YVO_4:Nd^{3+} ceramics: microstructural evolution and optical properties

LIHONG LIU, JIGUANG LI, KOJI MORITA, BYUNG-NAM KIM, AND TOHRU S. SUZUKI*

Research Center for Electronic and Optical Materials, National Institute for Materials Science, Tsukuba, Ibaraki 305-0047, Japan
Suzuki.tohru@nims.go.jp

Abstract: Enhanced optical properties of the (001) texture translucent YVO_4:Nd^{3+} ceramics can be achieved by adding $LiVO_3$ flux using a spark-plasma-sintering (SPS) technique. YVO_4:Nd^{3+} green body oriented along the (001) direction is successfully obtained from well-dispersed and highly stable YVO_4:Nd^{3+} suspension with suitable amount of $LiVO_3$ flux addition using 1wt% dispersant. The introduction of $LiVO_3$ flux can accelerate the sintering process and promote more effective densification during sintering. This ultimately leads to improved density of the YVO_4:Nd^{3+} ceramics compared to the sample without flux addition. The enhanced density, caused by the addition of the flux, finally results in the improved transmittance efficiency of the texture translucent YVO_4:Nd^{3+} ceramics.

1. Introduction

YVO_4 is an attractive host material for the rare earth ions, for its wide applications in solid state media for developing low and medium power micro-chip lasers with laser diode pumping due to its high absorption coefficient, high optical transparency in the 400-5000 nm range, large emission cross section, and long fluorescence lifetime [1–4]. Among them, YVO_4:Nd^{3+} crystals are especially desirable materials for diode pumped laser systems and deep space communication owing to their superiority over the widely used YAG:Nd^{3+} for their 2.7 times greater cross-section and higher slope efficiency compared with YAG:Nd^{3+} [5–7]. However, the traditional single-crystal growth method for producing high quality and large-sized YVO_4:Nd^{3+} crystals is costly, and the process is complex and difficult to control. As an alternative approach, the fabrication of transparent YVO_4:Nd^{3+} laser ceramics, which show higher c-cut thermal conductivity than that of YAG as reported by Taira et al. [8], offers a promising route to produce large-sized YVO_4:Nd^{3+} materials for using in high-power, high-efficiency laser designs. However, fabrication of transparent YVO_4:Nd^{3+} ceramic is quite challenging work due to the large birefringent scattering at the grain boundaries caused by its non-cubic crystal structure, along with the high melting point of YVO_4 (1810°C) [9]. To minimize light scattering losses at the grain boundaries of YVO_4, in our previous work, [10] aligning the crystal orientation of each grain, namely forming texture, was adopted by using strong magnetic field. By designing the (001) texture of YVO_4 with aligning the slip casting direction parallel to the magnetic field B the SPSed YVO_4 gained much higher transmittance than that of non-textured random YVO_4. The optical properties, however, are not determined only by one microstructural factor of the (001) texture, but also affected by other microstructural factors of the grain size and porosity [11,12]. Among them, the higher porosity in the sintering bodies would cause the serious light scattering, resulting in the poor transmittance of the final materials. To achieve high transparency in ceramics, it is important to eliminate porosity through proper material processing techniques, such as careful powder compaction, optimized sintering parameters, and the use of suitable

#574424 https://doi.org/10.1364/OE.574424
Journal © 2025 Received 4 Aug 2025; revised 11 Sep 2025; accepted 22 Sep 2025; published 20 Oct 2025

Optics EXPRESS

additives [13–15]. According to our previous works, [10] Y-rich impurity phase was detected in the YVO_4 ceramic after SPS sintering, which amount was increase with the increasing of sintering temperature. To consider the balance between impurity phase content and bulk density, a sintering temperature of 1300°C was ultimately chosen as the optimal temperature for producing translucent YVO_4 ceramic, even though some residual pores still exist in the ceramics. Aiming for even higher density necessitates subjecting the material to higher temperature processing. Nevertheless, this approach can result in the formation of a remarkable amount of impurity phases within the final products.

To overcome the drawbacks mentioned above, adding flux may become an effective method to enhance the density at lower temperature. A flux, characterized by its low melting point, can optimize the sintering process. In other words, introducing a flux can modify the sintering characteristics of the ceramic, making the sintering process more efficient. The flux can reduce the sintering temperature, accelerate particle bonding, and grain growth, thereby minimizing the formation of pores and defects and improving the density of the ceramic [16].

In this work, $LiVO_3$ with a melting point of 616 °C, typically used for preparing YVO_4 single crystal, which demonstrates low toxicity and volatility, [17] was selected as a flux to fabricate YVO_4:Nd^{3+} translucent ceramics. The colloidal technique [18–22] was employed to prepare a YVO_4:Nd^{3+} nanopowder suspension with good dispersion and stability by adding $LiVO_3$ flux. A magnetic field alignment technique [23–25] was proposed and applied using the slip casting method to create a (001) textured YVO_4:Nd^{3+} green body. Subsequently, the green body was sintered using the SPS technique, a powerful sintering tool capable of achieving high-density materials at relatively low temperatures, [26,27] to obtain translucent YVO_4:Nd^{3+} ceramics.

2. Experimental procedure

2.1. Preparation of YVO_4:Nd^{3+} nanopowder suspension

YVO_4:Nd^{3+} suspension was prepared from the nanopowders obtained using the same procedure as described in our previous works [10,28]. First, 15 vol% YVO_4:Nd^{3+} nanopowders were dispersed into distilled water; subsequently, 1 wt% $LiVO_3$ flux (Mitsuwa Chemical Co., Japan) was added to the suspension, followed by the addition of polyelectrolyte (poly(ammonium)acrylate A-6114, Toaghosei Co., Japan) as a dispersion medium to achieve a well-dispersed YVO_4:Nd^{3+} suspension. The adding amount of A-6114 was referred to 1wt% mass amount of YVO_4:Nd^{3+} in suspension. During the entire process, the pH value of the YVO_4:Nd^{3+} suspensions was adjusted to > 9 by Tetramethylammonium Hydroxide (TMAH). The suspension was then deagglomerated using a homogenizer for 10 minutes, followed by continuous stirring under ultrasonic dispersion for another 10 minutes.

2.2. Fabrication of textured-YVO_4 ceramic

The (001) textured-YVO_4:Nd^{3+} green body with flux addition was fabricated using slip casting in a strong magnetic field of 12 T, with the casting direction aligned parallel to the magnetic field. During the process, 4 mL of the prepared suspension was poured into an acryl tube mold with an inner diameter of 10.7 mm, which was fixed onto a porous Al_2O_3 substrate. The mold assembly was then placed inside the magnetic field chamber and subjected to the field for 24 hours to allow complete molding and orientation. The resulting slip-cast YVO_4:Nd^{3+} green compacts were subjected to cold isostatic pressing (CIP) at 350 MPa for 10 min and were then densified in a graphite mold using a SPS machine (SPS, LABOX-315, Sinterland Co., Ltd., Japan) at the sintering temperatures of T = 1300 °C with heating rates of 100 °C/min under a constant uniaxial pressure of 90 MPa. The pressure was increased to 90 MPa as the temperature rises from 1000 to 1100°C. The temperature during sintering was monitored by measuring the temperature of hole on the mold using an optical pyrometer.

Optics EXPRESS

2.3. Characterization techniques

Zeta-potential measurement of the suspension was performed as a function of flux adding amount by using zetasizer nano essentials (Malvern Instruments Ltd., United Kingdom).

X-ray diffraction (XRD) analysis of YVO_4:Nd^{3+} green bodies were performed by RINT-TTR-III diffractometer (Rigaku Co., Ltd, Tokyo, Japan, 40 kV 150 mA) using Cu Kα radiation. Electron backscatter diffraction (EBSD, EDAX-TSL OIM EBSD system, EDAX Inc., USA) characterization was conducted for texture analysis, which was performed using a field-emission scanning electron microscope (JSM7000F, JEOL Ltd., Tokyo, Japan). Orientation Imaging Microscopy TM (TexSEM Laboratories, Inc., Draper, UT) was used for collecting and analyzing the EBSD data. Microstructures of the ceramics were observed with a field emission scanning electron microscope (FE-SEM, model SU-8000, Hitachi Ltd., Tokyo, Japan). Using the SEM micrographs, the grain size was determined by counting the number of grains. Assuming the grains to be spherical, the average grain size, $\bar{d}$, was determined to be 1.225 times the apparent grain size, which was calculated from the average cross-sectional area per grain [29].

The transmittance efficiency in the wavelength range of $\lambda = 400$ -1400 nm were measured with the spectral resolution of 2 nm by using a double-beam spectrophotometer (SolidSpec-3700DUV, Shimadzu) equipped with an integrating sphere.

3. Results and discussion

3.1. Characterization of YVO_4:Nd^{3+} suspension

To consider the effect of flux adding amount on the dispersity of YVO_4:Nd^{3+} suspension, zeta potentials of YVO_4:Nd^{3+} suspensions with various $LiVO_3$ adding amounts were measured both before and after the addition of flux and A6114, respectively. For comparison, the zeta potential of YVO_4:Nd^{3+} suspension with only A6114 adding is also represented by the dark close-triangle. As shown in Fig. 1**,** the suspension exhibits a consistent, small positive zeta potential of approximately 2 mV before the addition of flux and A6114, and then the zeta potentials turn to the negative value of about −30, −40, −9 mV when 0.5 wt%, 1 wt%, and 2 wt% of $LiVO_3$ flux were respectively introduced into the suspension. After A6114 was added into the suspensions, the zeta potentials exceed > -40 mV for the suspensions containing 0.5 wt% and 1 wt% of $LiVO_3$, a similar value observed in suspension without flux addition. Whereas, the zeta potential of the suspension with 2 wt% $LiVO_3$ is slightly lower (−33 mV) than the others. This because normally, when suitable doping amount of flux was added into the suspension, charged groups adsorbed onto particle surfaces can impart more positive or negative charge to the particles, thereby increasing the zeta potential and improving stability. However, when the doping amount exceeds a certain level, adsorption sites on the particle surface become saturated, so additional additives cannot effectively adsorb and instead remain in the solution phase. These free additive molecules may compete with, displace, or "bridge" the molecules already adsorbed on the surface, which reduces the surface charge density. Consequently, the absolute value of the zeta potential decreases. Additionally, as the doping amount increases, the ionic strength of the solution rises, leading to compression of the electrical double layer (Debye layer). This compression reduces the effective transmission of surface charges into the surrounding solution. Thus, even if the actual surface charge remains relatively unchanged, the measured absolute zeta potential appears lower and the particles aggregate together, making rotation difficult and reducing the orientation degree. Although the zeta potential of the suspension with 2 wt% $LiVO_3$ is slightly lower than the others, the better colloidal stability can be achieved for the suspension with suitable amount of flux addition.

Optics EXPRESS

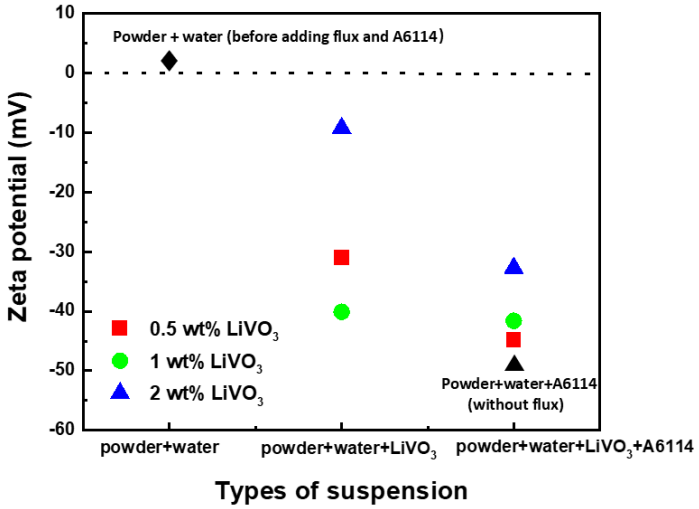

Fig. 1. Zeta potentials of YVO_4:Nd^{3+} suspensions with various $LiVO_3$ adding amounts measured both before and after the addition of $LiVO_3$ flux and A6114. For comparison, zeta potential of YVO_4:Nd^{3+} suspension without flux addition is also presented (closed black triangle).

3.2. *Characterization of crystalline orientation in YVO_4*

XRD patterns of YVO_4:Nd^{3+} green bodies with the addition of flux fabricated under the strong magnetic field of 12 T parallel to the slip casting direction are shown in Fig. 2**.** For comparison, the XRD pattern of the YVO_4:Nd^{3+} green body with the same orientation but without flux, as well as the XRD pattern of random YVO_4:Nd^{3+} green body with 1 wt% flux addition, are also presented. To make data comparison easier, the intensity of peak (112) in Fig. 2 was normalized to 1, and the intensities of other peaks were normalized relative to the intensity of peak (112) as well. The normalized reflection peak intensities of (004) and (200), which correspond to (001) and *a,b*-plane of YVO_4, respectively, are approximately employed to estimate the degree of orientation. Compared with the random sample, the relative intensity of (004) peak is enhanced, while the intensity (200) peak is correspondingly reduced in all the samples prepared under the magnetic field, indicating the (001) texture development in YVO_4:Nd^{3+} green bodies prepared under the strong magnetic field both with and without addition of $LiVO_3$ flux. Furthermore, YVO_4:Nd^{3+} samples with the addition of 0.5 wt% and 1 wt% flux exhibit a similar degree of orientation to that of the sample without flux addition. Although the orientation degree is lower in the sample with the addition of 2 wt% flux, due to the smaller zeta potential value of the suspension, the orientation in this case is significantly enhanced compared to the non-oriented sample as well. These experimental results suggest that the suitable addition amount of $LiVO_3$ flux does not have a detrimental effect on the orientation of the green body.

The well-textured green bodies with addition of flux obtained above were then sintered by SPS under 1300 °C with a fixed dwelling time of 10 min and heating rate of 100 °C/min under the pressure of 90 MPa. In order to examine the effect of flux addition on the shrinkage behavior of YVO_4:Nd^{3+}, the linear shrinkages during the sintering were recorded under the sintering temperature, as shown in Fig. 3**(a).** Before starting to apply the pressure at 1000 °C, as the temperature increases, the shrinkage occurs at around 850 °C for all the samples containing flux. In contrast, shrinkage starts at about 980 °C for the sample without flux addition, which is about 100 °C higher than that of the sample with flux addition. Figure 3(b) shows a comparison of the shrinkage rate (dL/dt) evaluated from the displacement L of Fig. 3(a)**.** Samples with the

Optics EXPRESS

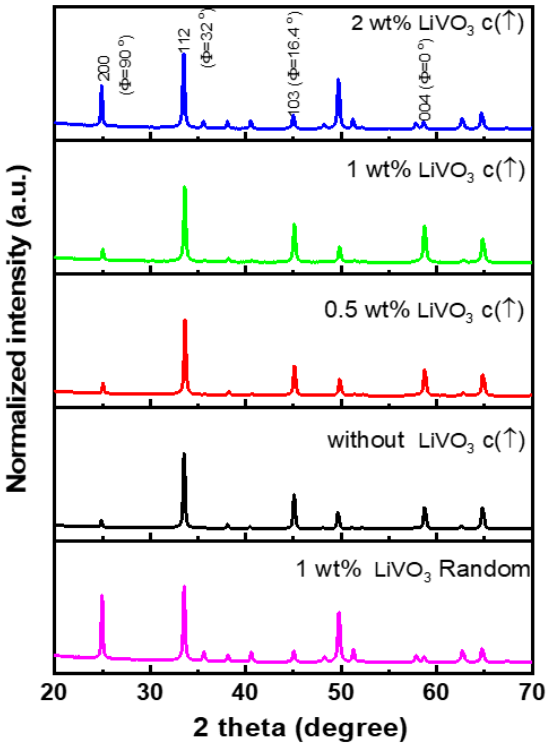

Fig. 2. XRD patterns of (001) textured-YVO_4:Nd^{3+} green body with various flux additions. For comparison, the XRD patterns of the textured-YVO_4:Nd^{3+} without flux addition and the random YVO_4:Nd^{3+} with 1 wt% flux addition are also presented.

addition of flux exhibit a pronounced shrinkage slope around 925°C, a temperature significantly lower than the corresponding point for the sample without flux addition (which occurs at around 1025°C). This discrepancy is a result of the significant impact that flux exerts on the sintering process. That is, flux can form a liquid phase during sintering, it allows particles to rearrange and bond together at lower temperatures; also, the liquid phase created by flux improves particle mobility, enabling particles to move and densify more effectively during sintering, which can lead to improved densification processing of the sample [30].

Texture structures of SPSed-YVO_4:Nd^{3+} with and without added flux were characterized using the SEM-EBSD technique. Figures 4 shows the EBSD inverse pole figure (IPF) maps for the YVO_4:Nd^{3+} without and with 1 wt% flux addition. The surface perpendicular to the applying direction of the magnetic field was analyzed and colored by the color code on the standard stereographic triangle shown in Fig. 4.

In Fig. 4(b)**,** for the sample with 1 wt% flux addition, most grains exhibit red and red-orange colors, similar in orientation to the sample without flux addition (Fig. 4**(a)),** suggesting that well-orientated (001) planes can be obtained with the addition of 1 wt% flux. This result demonstrates that the (001) textured structure can successfully be achieved by controlling the flux addition.

The detailed degree of the (001) texture in YVO_4:Nd^{3+} with and without adding flux can be illustrated from the distributions of the tilt angle between the *c*-axis and the vertical direction. These distributions can be calculated by using the multiples of a random distributions (MRD) from the EBSD data, as shown in Fig. 5. The distribution f_{MD} of the *c*-axis in the YVO_4:Nd^{3+}

Optics EXPRESS

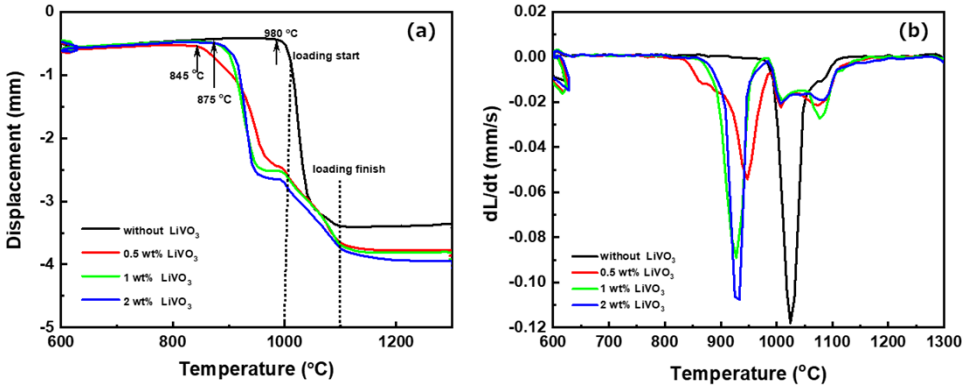

Fig. 3. (a) Punch displacement L as functions of the sintering temperature T, (b) densification rate (dL/dt) as a function of the sintering temperature T for the samples fabricated with and without $LiVO_3$ flux addition.

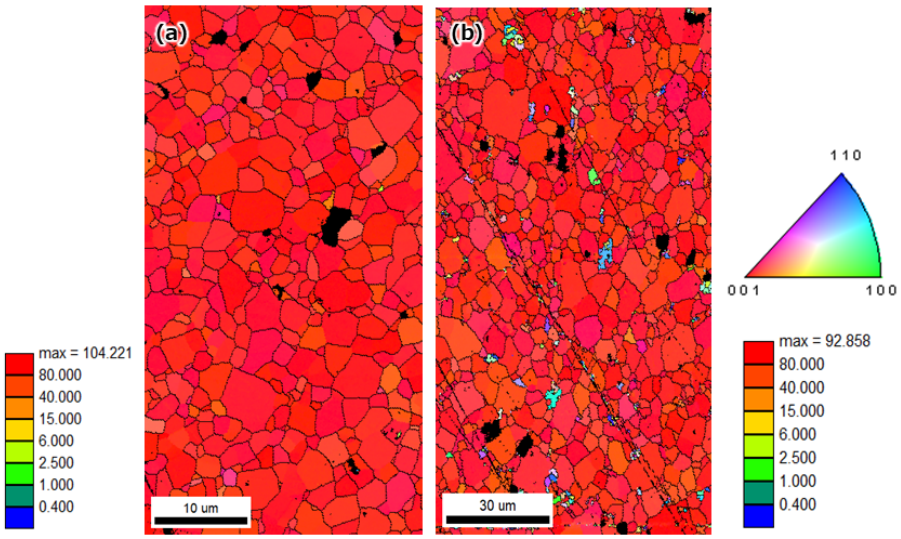

Fig. 4. EBSD inverse pole figure (IPF) mappings of the SPSed-YVO_4:Nd^{3+} without (a), and with 1 wt% (b) $LiVO_3$ flux addition. Corresponding pole figures were inserted at the bottom of each IPF maps.

with and without adding flux is plotted against the tilting angle (θ) between the c-axis and the vertical direction. For samples without and with various flux additions, f_{MD} shows a peak around $\theta = 0°$. This suggests that approximately 94.2%, 92.7%, 91.8%, and 61.4% of grains have (001) planes aligned within the tilting angle $\theta<10°$ for YVO_4:Nd^{3+} without and with flux additions of 0.5%, 1%, and 2% wt, respectively. Although the sample with 2 wt% flux addition shows a lower degree of orientation, the results indicate that adding 0.5 and 1 wt% flux to YVO_4:Nd^{3+} has no significant detrimental effect on the orientation degree of the samples.

Figure 6 gives the microstructures of YVO_4:Nd^{3+} both with and without flux addition. It is clearly demonstrated that the introduction of flux leads to a corresponding increase in the grain size of YVO_4:Nd^{3+}. As compared with grain size of the sample without flux addition (3.17 μm), for the YVO_4:Nd^{3+} fabricated from the green body with added 0.5 wt% flux, exhibits

Optics EXPRESS

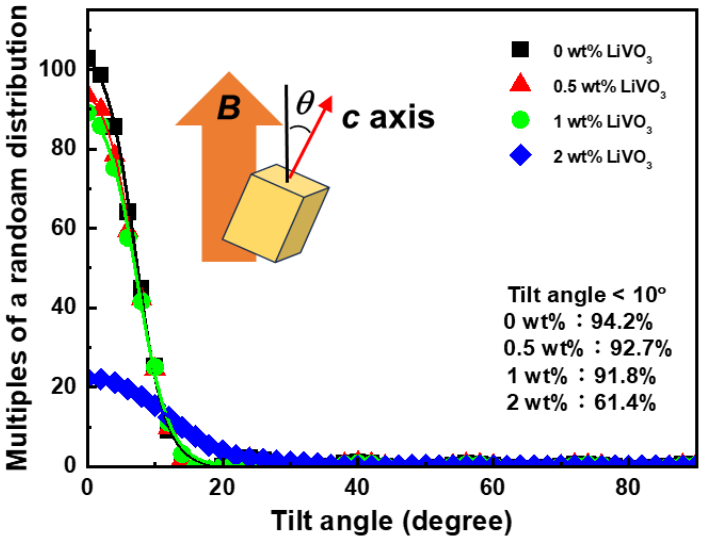

Fig. 5. c-axis distribution in the SPSed-YVO_4:Nd^{3+} without and with various flux additions.

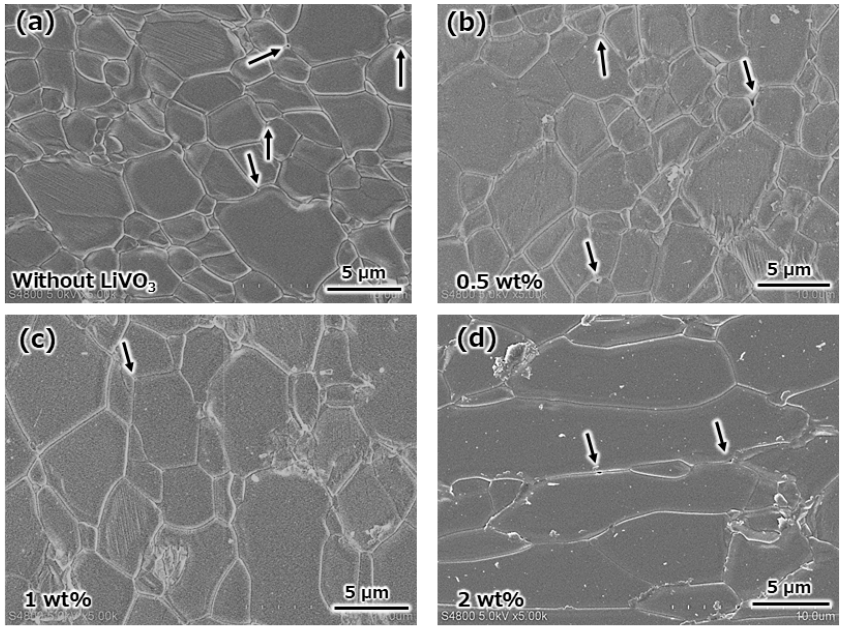

Fig. 6. SEM images of (001) textured-YVO_4:Nd^{3+} ceramics fabricated at 1300 °C with a constant dwelling time of 10 min and a heating rate of 100 °C/min, without flux (a), and with 0.5 wt% (b), 1 wt% (c), and 2 wt% (d) $LiVO_3$ flux additions.

an average grain size of approximately 3.71 μm. Similarly, when the flux addition amount is increased to 1 wt%, the average grain size further grows to about 4.8 μm. The largest grain size (10.32μm) is achieved in the sample with 2 wt% flux addition. This is because flux increases the mobility of atoms or ions within the material, making it easier for them to diffuse and reposition themselves during sintering. This increased mobility facilitates the grain boundary migration

Optics EXPRESS

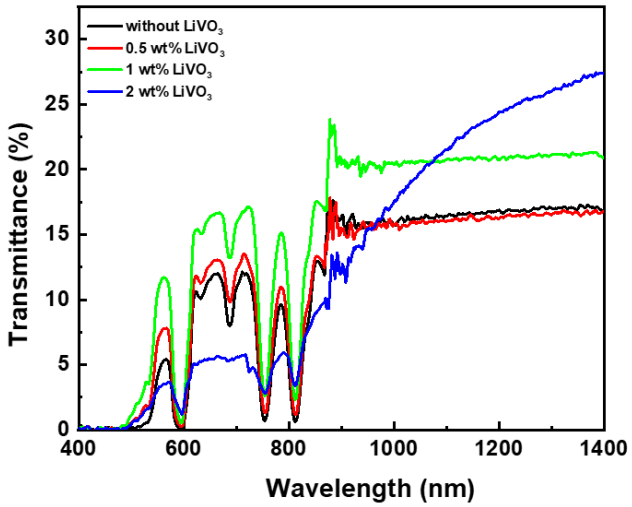

Fig. 7. Transmittance efficiencies of the (001) textured-YVO_4:Nd^{3+} ceramics fabricated with and without $LiVO_3$ flux addition.

and coalescence, finally lead to large grain size of the sample. In addition, the density of the sample can be enhanced by adding flux (Fig. 6), the residual pores at the multiple grain junctions can be reduced as flux addition. During sintering, flux can form liquid phase which facilitates particle rearrangement and bonding, resulting in improved densification. The flux also acts as a "liquid bridge" between particles, promoting better packing and reducing the number of pores in the sintered material.

3.3. Optical properties of (001) textured-YVO_4:Nd^{3+} ceramics

Figure 7 displays the transmittance efficiencies of textured-YVO_4:Nd^{3+} with 1wt% and without flux addition in the wavelength range from the visible to near-IR wavelength of $\lambda = 400$ -1400 nm. Notably, distinct absorption peaks at about the wavelength of 590, 680, 750, and 810 nm can be observed in both samples owing to the Nd^{3+} doping. The uneven profile around the wavelength of 900 nm is due to the equipment and does not reflect the properties of the sample. The impact of flux addition on transmittance is significant, the sample with 1 wt% flux addition displays markedly higher transmittance compared to the textured sample without flux under identical sintering conditions, at the whole measurement wavelength range. For YVO_4 with a non-cubic crystal structure, transmittance is known to be greatly influenced by microstructural factors such as texture, grain size, and porosity. The textured-YVO_4:Nd^{3+} ceramics both with 1 wt% and without flux addition exhibit the similar orientation degree, as observed in Fig. 4. Thus, grain size and porosity may the main factors causing the different transmittance in these two samples. Normally, the larger the grain size, the greater the interaction of light within the material, resulting in significant effects such as scattering, absorption, multiple reflections, and refractions, ultimately leading to reduced transmittance. However, YVO_4:Nd^{3+} with 1 wt% flux addition, which shows the larger grain size (4.8 μm) than that of the sample without adding flux (3.17 μm), display the higher transmittance, deducing that increased density resulting from flux addition is expected to play an important role for increasing the enhanced transmittance efficiency. In addition, the amount of liquid phase generated during sintering with 0.5 wt% flux addition is limited and insufficient to eliminate pores. Consequently, the reduction in light scattering is only partial, resulting in a modest improvement in visible transmittance compared to the flux-free sample. In the long-wavelength range, however, the dominant loss mechanism is Mie scattering.

Optics EXPRESS

Since the pores in this sample remain at the micrometer scale, the scattering intensity remains nearly unchanged, leading to transmittance values comparable to those of the flux-free sample. In contrast, for the sample with 2 wt% flux addition, the excess liquid phase may form residual Li–V-rich glassy films at grain boundaries, which can introduce absorption or color centers in the visible wavelength range. Nevertheless, the pores are effectively healed, thereby minimizing long-wavelength scattering and yielding high near-IR transmittance in this sample.

4. Conclusions

Enhanced optical properties of (001) textured translucent YVO_4:Nd^{3+} ceramics can be achieved by introduction of $LiVO_3$ flux using the SPS technique. Similar to the sample without the addition of flux, the introduction of flux with the amount less than 1 wt% to the sample also allows for the achievement of a well-dispersed suspension and a high degree of orientation in the green body, indicating that the addition of $LiVO_3$ flux with suitable amount does not have a detrimental effect on the dispersity of the suspension and the orientation of the green body. During the SPS sintering process, the introduction of $LiVO_3$ flux can promote more effective densification during sintering via the liquid phase created. This ultimately leads to improved density of the YVO_4:Nd^{3+} ceramics compared to the sample without flux addition, and finally results in the enhanced transmittance of the YVO_4:Nd^{3+} ceramics. These results demonstrate that controlling the microstructure by introduction suitable amount of flux using a textured structure method is a suitable way to enhance the transmittance of YVO_4:Nd^{3+} ceramics.

Funding. Innovative Science and Technology Initiative for Security (JPJ004596).

Acknowledgements. The part of this work was financially supported by Innovative Science and Technology Initiative for Security, Grant Number JPJ004596, ATLA, Japan.

Disclosures. The authors declare no conflicts of interest.

Data availability. Data underlying the results presented in this paper are not publicly available at this time but may be obtained from the authors upon reasonable request.

References

1. H. K. Yang, H. Choi, B. K. Moon, *et al.*, "Improved luminescent behavior of YVO_4: Eu^{3+} ceramic phosphors by Li contents," Solid State Sci. **12**(8), 1445–1448 (2010).
2. T. Taira, A. Mukai, Y. Nozawa, *et al.*, "Single-mode oscillation of laser-diode-pumped Nd : YVO_4 microchip lasers," Opt. Lett. **16**(24), 1955–1957 (1991).
3. S. Zhang, X. Wu, X. Yan, *et al.*, "Effects of CaO addition on growth of YVO_4 single crystals," J. Cryst. Growth **247**(3-4), 428–431 (2003).
4. B. Q. Hu, Y. Z. Zhang, X. Wu, *et al.*, "Defects in large single crystals Nd: YVO_4," J. Cryst. Growth **226**(4), 511–516 (2001).
5. X. Meng, L. Zhu, H. Zhang, *et al.*, "Growth, morphology and laser performance of Nd: YVO_4 crystal," J. Cryst. Growth **200**(1-2), 199–203 (1999).
6. R. A. Fields, M. Birnbaum, and C. L. Fincher, "Highly efficient Nd: YVO_4 diode-laser end-pumped laser," Appl. Phys. Lett. **51**(23), 1885–1886 (1987).
7. Y. Kuwano and S. Saito, "Nd: YVO_4 single crystal for LD pumped solid state laser," Rev. Laser Eng. **18**(8), 616–621 (1990).
8. Y. Sato and T. Taira, "The studies of thermal conductivity in $GdVO_4$, YVO_4, and $Y_3Al_5O_{12}$ measured by quasi-one-dimensional flash method," Opt. Express **14**(22), 10528–10536 (2006).
9. K. Chow and H. G. McKnight, "The growth and characterization of pure and rare-earth-substituted YVO_4," Mater. Res. Bull. **8**(12), 1343–1350 (1973).
10. L. H. Liu, J. G. Li, K. Morita, *et al.*, "Enhanced optical properties of translucent YVO_4 ceramic fabricated by spark-plasma-sintering (SPS) via texture-controlled microstructure," Opt. Express **33**(8), 16976–16986 (2025).
11. L. H. Liu, K. Morita, T. S. Suzuki, *et al.*, "Effect of volume ratio on optical and mechanical properties of Y_2O_3-MgO composites fabricated by spark-plasma-sintering process," J. Eur. Ceram. Soc. **41**(3), 2096–2105 (2021).
12. L. H. Liu, K. Morita, T. S. Suzuki, *et al.*, "Evolution of microstructure, mechanical, and optical properties of Y_2O_3-MgO nanocomposites fabricated by high pressure spark plasma sintering," J. Eur. Ceram. Soc. **40**(13), 4547–4555 (2020).
13. S. F. Wang, J. Zhang, D. W. Luo, *et al.*, "Transparent ceramics: Processing, materials and applications," Prog. Solid State Chem. **41**(1-2), 20–54 (2013).

Optics EXPRESS

14. O. Guillon, J. Gonzalez-Julian, B. Dargatz, *et al.*, "Field-assisted sintering technology/spark plasma sintering: mechanisms, materials, and technology developments," Adv. Eng. Mater. **16**(7), 830–849 (2014).
15. K. Morita, B. N. Kim, H. Yoshida, *et al.*, "Spark-plasma-sintering condition optimization for producing transparent $MgAl_2O_4$ spinel polycrystal," J. Am. Ceram. Soc. **92**(6), 1208–1216 (2009).
16. S. Chen and D. G. Zhu, "Low-temperature densification sintering and properties of $CaAl_2Si_2O_8$ ceramics with $MeO \cdot 2B_2O_3$ (Me = Ca, Sr, Ba)," Int. J. Miner. Process. **22**(9), 977–986 (2015).
17. S. Erdei, "Growth of oxygen deficiency-free YVO_4 single crystal by top-seeded solution growth technique," J. Cryst. Growth **134**(1-2), 1–13 (1993).
18. H. Windlass, P. M. Raj, D. Balaraman, *et al.*, "Colloidal processing of polymer ceramic nanocomposite integral capacitors," IEEE Trans. Electron. Packag. Manuf. **26**(2), 100–105 (2003).
19. M. Suárez, A. Fernández, J. L. Menéndez, *et al.*, "Hot isostatic pressing of optically active Nd: YAG powders doped by a colloidal processing route," J. Eur. Ceram. Soc. **30**(6), 1489–1494 (2010).
20. J. Sun, L. Gao, and W. Li, "Colloidal processing of carbon nanotube/alumina composites," Chem. Mater. **14**(12), 5169–5172 (2002).
21. T. S. Suzuki, T. Uchikoshi, and Y. Sakka, "Control of texture in alumina by colloidal processing in a strong magnetic field," Sci. Technol. Adv Mat. **7**(4), 356–364 (2006).
22. F. F. Lange, "Colloidal processing of powder for reliable ceramics," Curr. Opin. Solid St. M. **3**(5), 496–500 (1998).
23. T. S. Suzuki, "Advanced control of crystallographic orientation in ceramics by strong magnetic field," J. Ceram. Soc. Jpn. **128**(12), 1005–1012 (2020).
24. T. Ashikaga, B. N. Kim, H. Kiyono, *et al.*, "Effect of crystallographic orientation on transparency of alumina prepared using magnetic alignment and SPS," J. Eur. Ceram. Soc. **38**(7), 2735–2741 (2018).
25. T. S. Suzuki, T. Uchikoshi, and Y. Sakka, "Effect of sintering additive on crystallographic orientation in AlN prepared by slip casting in a strong magnetic field," J. Eur. Ceram. Soc. **29**(12), 2627–2633 (2009).
26. L. H. Liu, K. Morita, T. S. Suzuki, *et al.*, "Synthesis of highly-infrared transparent Y_2O_3–MgO nanocomposites by colloidal technique and SPS," Ceram. Int. **46**(9), 13669–13676 (2020).
27. S. Grasso, H. Yoshida, H. Porwal, *et al.*, "Highly transparent α-alumina obtained by low cost high pressure SPS," Ceram. Int. **39**(3), 3243–3248 (2013).
28. S. Huang, X. Wang, Q. Zhu, *et al.*, "Systematic synthesis of $REVO_4$ micro/nano crystals with selective exposure of high energy {001} facets and luminescence (RE = Lanthanide and $Y_{0.95}Eu_{0.05}$)," J. Mater. Res. Technol. **9**(6), 12547–12558 (2020).
29. R. Apetz and M. P. V. Bruggen, "Transparent alumina: a light-scattering model," J. Am. Ceram. Soc. **86**(3), 480–486 (2003).
30. C. Sun, X. Wang, C. Ma, *et al.*, "Low-Temperature Sintering Barium Titanate-Based X8R Ceramics with Nd_2O_3 Dopant and ZnO–B_2O_3 Flux Agent," J. Am. Ceram. Soc. **92**(7), 1613–1616 (2009).